

# Low temperature spectrum of a fiber loop laser

Eyal Buks<sup>1,\*</sup>

<sup>1</sup>Andrew and Erna Viterbi Department of Electrical Engineering, Technion, Haifa 32000 Israel  
(Dated: December 6, 2022)

Fiber-based multi-wavelength lasers have a variety of important applications in telecommunication and meteorology. We experimentally study a fiber loop laser with an integrated Erbium doped fiber (EDF). The output optical spectrum is measured as a function of the EDF temperature. We find that below a critical temperature of about 10K the measured optical spectrum exhibits a sequence of narrow and unequally-spaced peaks. An intriguing connection between the peaks' wavelengths and the sequence of prime numbers is discussed. An hypothesis, which attributes the comb formation to intermode coupling, is explored.

**Introduction** - Erbium doped fibers (EDF) are widely employed in a variety of applications. Key properties of EDF can be controlled by varying the temperature. The contribution of Brillouin scattering [1] to the temperature dependency has been explored in [2–6].

In this work we study a fiber loop laser with an integrated EDF [7, 8]. We measure the emitted optical spectrum as a function of the EDF temperature [9, 10]. Below a critical temperature of about 10K the measured optical spectrum exhibits an unequally-spaced optical comb (USOC) made of a sequence of narrow peaks. We discuss a possible connection between the observed USOC and intermode coupling [11]. Theoretical modeling is employed to explore this connection. The parameters characterizing intermode coupling are extracted from open loop measurements.

**Experimental setup** - The experimental setup is schematically depicted in the inset of Fig. 1. EDF having length of 20m, absorption of  $30 \text{ dB m}^{-1}$  at 1530nm, and mode field diameter of  $6.5 \mu\text{m}$  at 1550nm, is cooled down using a cryogen free cryostat. The EDF is thermally coupled to a calibrated silicon diode serving as a thermometer, and it is pumped using a 980nm laser diode (LD) biased with current denoted by  $I_D$ . The cold EDF is integrated with a room temperature fiber loop using a wavelength-division multiplexing (WDM) device. Two isolators (labeled by arrows in the sketch shown in Fig. 1) and a 10:90 output coupler (OC) are integrated in the fiber loop. The loop frequency  $f_L$  (inverse loop period time), which is measured using a radio frequency spectrum analyzer and a photodetector, is given by  $f_L = c/(n_F l_L) = 4.963 \text{ MHz}$ , where  $c$  is the speed of light in vacuum,  $n_F = 1.45$  is the fiber refractive index (in the telecom band), and  $l_L = 41.7 \text{ m}$  is the fiber loop total length. An optical spectrum analyzer (OSA) is connected to the 10:90 OC.

**Temperature dependence** - The measured optical spectrum as a function of the temperature  $T$  with diode current of  $I_D = 200 \text{ mA}$  ( $I_D = 120 \text{ mA}$ ) is shown in Fig. 1 (Fig. 2). The low temperature lasing threshold occurs at

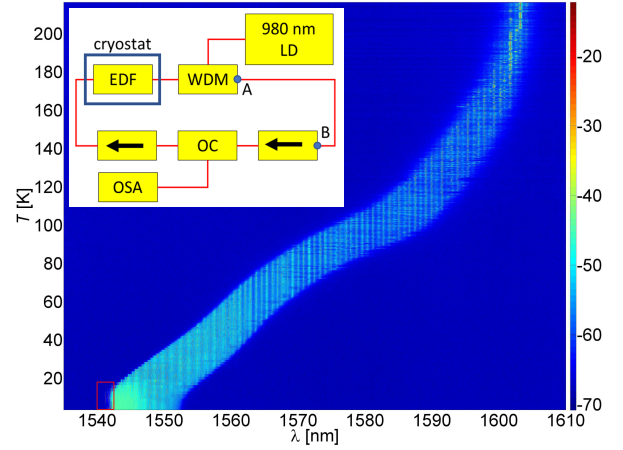


FIG. 1: The measured optical spectrum in dBm units as a function of the wavelength  $\lambda$  and the temperature  $T$  with diode current of  $I_D = 200 \text{ mA}$ . The corresponding diode voltage and diode optical power are 1.38V and 0.044W, respectively. The overlaid red rectangle indicates the region shown in higher resolution in Fig. 2. The experimental setup is shown in the inset. The EDF is inside the cryostat, and all other components are at room temperature. The isolator on the right was added to block back-reflected light from the OSA input port.

$I_D = 88 \text{ mA}$  [see Fig. S1 of the supplementary materials (SM)].

The optical spectrum shown in Fig. 1 reveals a transition from the short to the long EDF limits. The wavelength at which lasing peaks is denoted by  $\lambda_g$ . The spectrum shown in Fig. 1 indicates that  $\lambda_g$  decreases as the temperature is lowered [12], from 1605nm at room temperature, to 1540nm below 10K.

It was shown in Ref. [13] that the wavelength  $\lambda_g$  can be determined by finding the value of  $\lambda$  that maximizes the dimensionless variable  $\eta$ , which is given by

$$\eta = \frac{1 - \frac{1}{z_E^{-1} z_{Fe}}}{1 + \frac{z_A^{-1}}{z_E^{-1}}}, \quad (1)$$

where  $z_E^{-1}$  ( $z_A^{-1}$ ) is the emission (absorption) inverse

\*eyal@ee.technion.ac.il

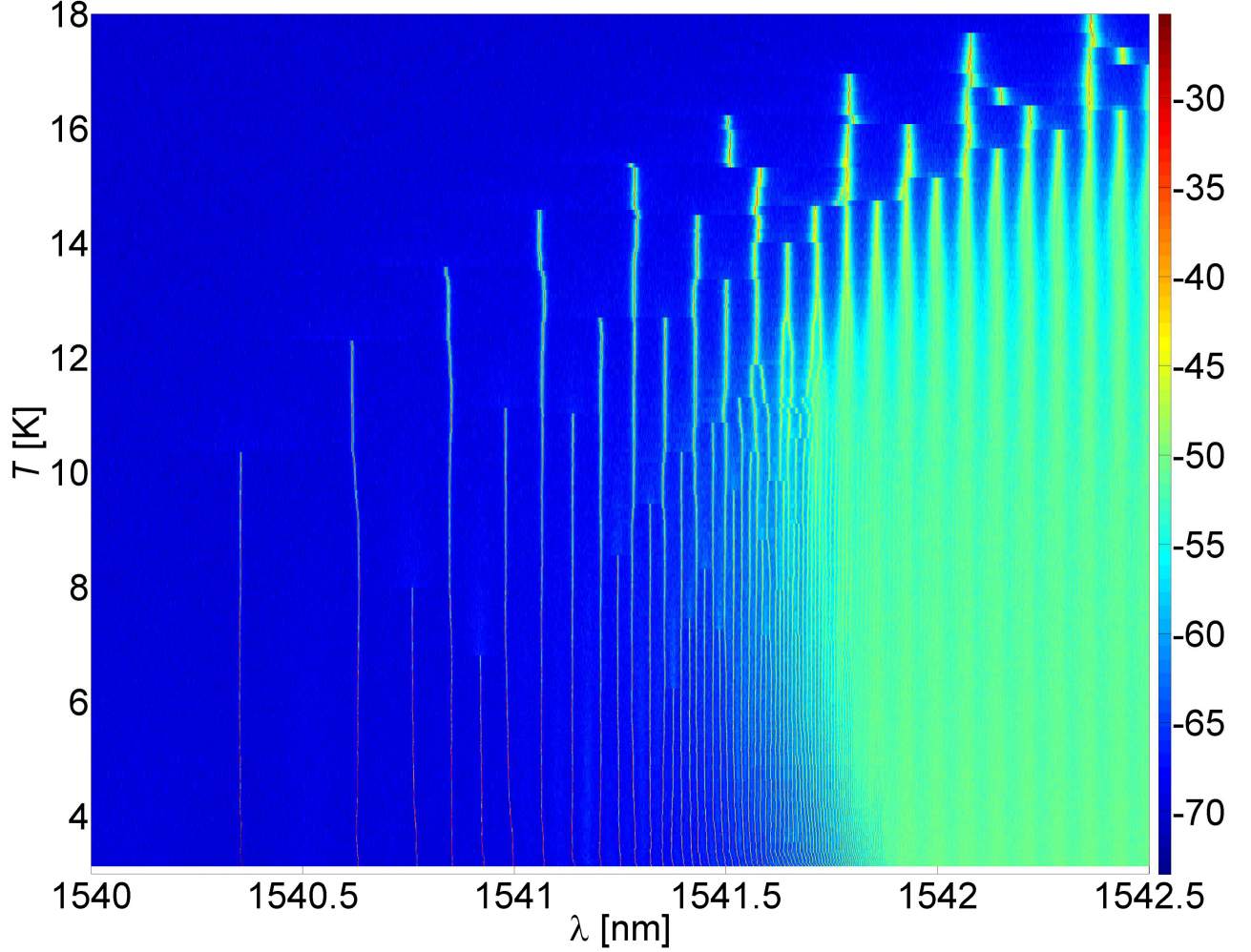


FIG. 2: The optical spectrum in dBm units below 18K. Diode current for this measurement is  $I_D = 120\text{mA}$ .

length at wavelength  $\lambda$ , and  $z_{\text{Fe}} = z_F / \log \gamma_L$  represents an effective value for the EDF length  $z_F$ , where  $\gamma_L \geq 1$  is the loop loss coefficient, which is mainly determined by the output coupler splitting ratio. In thermal equilibrium the ratio  $z_A^{-1}/z_E^{-1}$  at wavelength  $\lambda$  is given by the Einstein (McCumber) relation  $z_A^{-1}/z_E^{-1} = e^{-\rho}$ , where  $\rho = \lambda_T (\lambda_0^{-1} - \lambda^{-1})$ ,  $\lambda_0$  is the wavelength for which  $z_A^{-1} = z_E^{-1}$ ,  $\lambda_T = hc / (n_F k_B T)$  is the thermal wavelength, where  $h$  is the Planck's constant,  $k_B$  is the Boltzmann's constant, and  $T$  is the temperature.

The relative importance of the term  $1 / (1 + z_A^{-1}/z_E^{-1}) \equiv f$  in Eq. (1) depends on the ratio  $z_E^{-1}/z_{\text{Fe}}$  between the effective EDF length  $z_{\text{Fe}}$  and the emission length  $z_E$ . In the long EDF limit (i.e. when  $z_E^{-1}/z_{\text{Fe}} \gg 1$ ) the term  $f$  has a relatively large influence on the lasing wavelength  $\lambda_g$ . In our experiment, the long EDF limit corresponds to temperatures above 200K, for which  $\lambda_g \simeq 1605\text{nm}$  (see Fig. 1). At this value of  $\lambda_g$  absorption is strongly suppressed, i.e.  $z_A^{-1} \ll z_E^{-1}$ , and

consequently a relatively large value for  $f$  is obtained. In the opposite limit of low temperatures below 10K, the ratio  $z_E^{-1}/z_{\text{Fe}}$  decreases, and consequently the lasing band is shifted to the region where emission cross section peaks near  $\lambda_g \simeq 1540\text{nm}$  (see Fig. 1) [14–16].

Near wavelength of 1540nm and below a critical temperature of about 10K the measured optical spectrum exhibits narrow peaks at a sequence of wavelengths denoted by  $\{\lambda_k\}$ , where  $k = 0, 1, 2, \dots$  [see Fig. 2 and Fig. 3(a)]. For the data presented in Fig. 3(a)  $\lambda_0 = 1540.5039\text{nm}$  and  $\lambda_1 - \lambda_0 = 0.1875\text{nm}$ . The frequency  $f_k$  associated with wavelength  $\lambda_k$  is given by  $f_k = c/\lambda_k$ . For the smallest wavelength spacings that can be reliably resolved  $\lambda_{k+1} - \lambda_k \simeq 1.7\text{pm}$  and  $f_{k+1} - f_k \simeq -200\text{MHz}$ , with  $k \simeq 150$ . The frequency associated with the gap between  $\lambda_0$  and  $\lambda_1$  is given by  $f_1 - f_0 = 23.69\text{GHz}$ .

A plot of the dimensionless sequence  $i_k = (f_0 - f_k) / f_L$  is shown in Fig. 3(b). This sequence is further explored in the SM. In particular, Eq. (S14) of the SM reveals

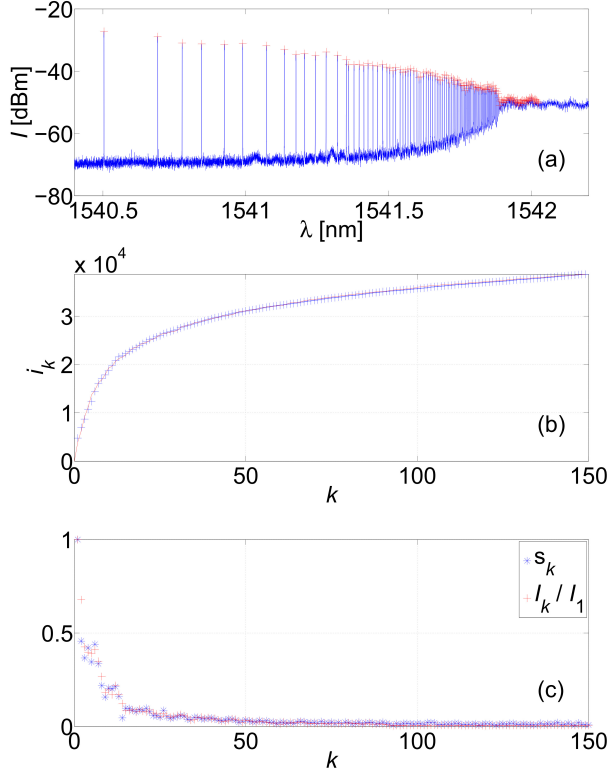


FIG. 3: The USOC sequence. The LD is biased with a current of  $I_D = 120\text{mA}$ . (a) The optical spectrum (measured by the OSA) at the base temperature of 3K. (b) Comparison between the measured values of the dimensionless sequence  $i_k = (f_0 - f_k)/f_L$  (crosses), and the values of  $n_k$  calculated using Eq. (S14) of the SM (solid line). (c) The normalized wavelength gaps  $s_k = (\lambda_k - \lambda_{k-1})/(\lambda_1 - \lambda_0)$  (stars) and the USOC measured normalized intensities  $I_k/I_1$  (crosses) as a function of  $k$ .

an intriguing connection between  $i_k$  and the sequence of prime numbers.

The intensity of the USOC peak occurring at wavelength  $\lambda_k$  is denoted by  $I_k$ . The plot in Fig. 3(c) compares the USOC measured normalized wavelength gaps  $s_k = (\lambda_k - \lambda_{k-1})/(\lambda_1 - \lambda_0)$  and the USOC measured normalized intensities  $I_k/I_1$ . The comparison indicates that to a good approximation  $s_k = I_k/I_1$ , i.e. the ratio  $(\lambda_k - \lambda_{k-1})/I_k$  is nearly a constant.

No change in the measured optical spectrum is detected when a magnetic field up to 0.15T is externally applied. Note that strong effect of magnetic field on the optical decoherence rate in an EDF was found at low temperatures using the method of two-pulse photon echoes [17, 18].

**Open loop** - Open loop measurements are performed by disconnecting the fiber between the points labeled as 'A' and 'B' in the inset of Fig. 1, connecting OSA to 'A' and an optical source to 'B'. As is discussed below, open loop measurements allow the characterization

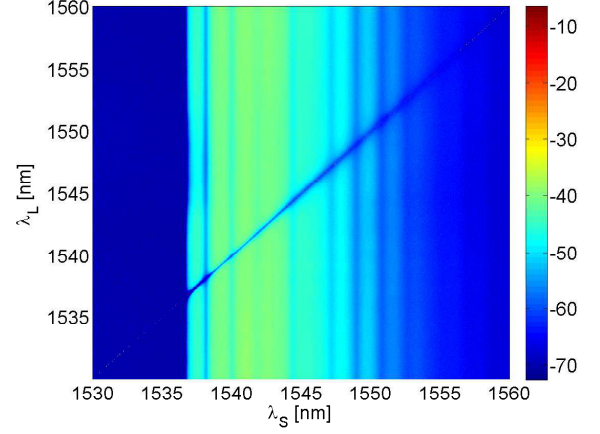


FIG. 4: Open loop gain. The transmitted light optical spectrum is shown in dBm units as a function of the tunable laser wavelength  $\lambda_L$ . Tunable laser linewidth is 1.6pm, its power is  $-4.1$  dBm, the temperature is  $T = 2.9\text{K}$ , diode current is  $I_D = 150\text{mA}$ , and its optical linewidth is about 1nm.

of EDF gain and intermode coupling.

For the measurements shown in Fig. 4 the source connected to 'B' is a narrow band laser having a tunable wavelength  $\lambda_L$ . The measured transmitted light optical spectrum is shown in Fig. 4 as a function of  $\lambda_L$ . The signal suppression near  $\lambda_L$  is attributed to the effects of gain saturation and hole burning [19]. A similar measurement performed with a closed loop is presented by Fig. S2 of the SM.

Intermode coupling can be explored using the method of intermodulation (IMD). This is done by injecting two monochromatic tones into the system under study. The first one, which has a relatively large amplitude, and a wavelength denoted by  $\lambda_p$ , is commonly referred to as the *pump*. The second one is a relatively low-amplitude *signal* tone having wavelength  $\lambda_s = \lambda_p - \lambda_d$ , where  $\lambda_d$  is the detuning wavelength, which is assumed to be small  $|\lambda_d| \ll \lambda_p$ . Nonlinear frequency mixing can be characterized by measuring the response at the *idler* wavelength  $\lambda_i = \lambda_p + \lambda_d$ . For the IMD measurements presented in Fig. 5, an optical modulator based on a ferrimagnetic sphere resonator (FSR) is employed [20]. This device can generate single sideband modulation provided that the input polarization (of the laser light injected into the FSR) is properly tuned [see Fig. 5(a)] [20]. Frequency mixing between the pump and signal input tones occurring in the EDF gives rise to an idler tone at the output. The idler peak can be detected in the transmitted light optical spectrum when the diode current  $I_D$  is tuned above its threshold value [see Fig. 5(b)]. The measured idler intensity allows the extraction of IMD gain of the medium, which, in turn, determines the intermode coupling rates.

**Equations of motion** - Intermode coupling is theoretically explored by deriving equations of motion. The



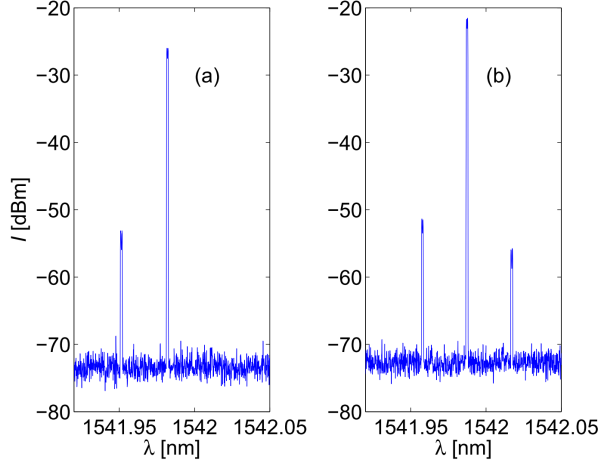


FIG. 5: Open loop IMD. The transmitted light optical spectrum (a) below threshold  $I_D = 94\text{mA}$ , and (b) above threshold  $I_D = 144\text{mA}$ . The laser power is 14.9 dBm, the laser wavelength is 1541.982nm, the temperature is  $T = 2.9\text{K}$ , the FSR modulator driving frequency is 3.792GHz, and the corresponding optical sideband wavelength detuning is  $\lambda_d = 30\text{pm}$ .

(assumed slowly varying) complex amplitude of the fiber loop  $m$ 'th mode is denoted by  $c_m$ . Consider the case where the time evolution of  $c_m$  is governed by [21]

$$\dot{c}_m = \Gamma_d m^2 c_m - \Gamma_c V_m + g_m c_m, \quad (2)$$

where overdot denotes a time derivative, both the dispersion rate  $\Gamma_d = \Gamma'_d + i\Gamma''_d$  and coupling rate  $\Gamma_c = \Gamma'_c + i\Gamma''_c$  are complex ( $\Gamma'_d, \Gamma''_d, \Gamma'_c$  and  $\Gamma''_c$  are all real), and where the interaction term  $V_m$  is given by

$$V_m = \sum_{n'-n''+n'''=m} c_{n'} c_{n''}^* c_{n'''} . \quad (3)$$

Due to strong temperature dependency of line-widths of optical transitions in the EDF [22], multimode lasing becomes possible at low temperatures [8, 23]. This is taken into account by allowing the gain  $g_m$  in the master equation (2), which is commonly assumed to be mode-independent, to vary with  $m$ . The assumed dependency is given by  $g_m = (1 + g_0) / (1 + H_m/I_{\text{sat}}) - 1$ , where  $g_0$  is the low intensity gain, and  $I_{\text{sat}}$  is the saturation intensity. The open loop gain measurements [see Fig. 4] can be well fitted to  $g_m$  when the effective  $m$ 'th intensity  $H_m$  is taken to be given by  $H_m = \sum_n h_{n,m} |c_n|^2$ , where  $h_{n,m} = \delta_{n,m} + \alpha_H (1 - \delta_{n,m}) |n - m|^{-1}$ , and  $\alpha_H$  is a positive constant. For this effective intensity  $H_m$ , the hole that is burned by a single excited mode having amplitude  $c_n$  contains about  $\alpha_H I_{\text{sat}}^{-1} |c_n|^2$  modes. The value of  $\Gamma_c$  is determined from IMD measurements [see Fig. 5].

A numerical solution example for the coupled equations (2) is shown in Fig. 6. For this example, the gap between peaks (in units of spacing between neighboring

modes) varies from about 70 (near  $n = 0$ ) to about 2 (near  $n = 1000$ ), where  $n$  denotes the mode index number. This example demonstrates that this simple model can account for a spontaneous generation of a USOC. However, further study is needed to explore the temperature dependency of the model's parameters, in order to account for the experimental observation that the USOC becomes visible only below the critical temperature of about 10K.

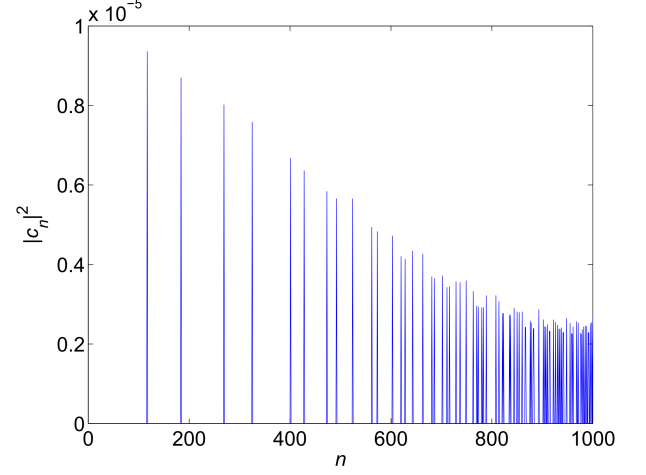


FIG. 6: Numerical solution of the set of coupled equations (2). The mode index number is denoted by  $n$ . For this example the total number of modes is 1000,  $\Gamma_d = 10^{-7} \times (1 + 0.1i)$ ,  $\Gamma_c = 0.05$ ,  $g_0 = 1.2$ ,  $I_{\text{sat}} = 10^{-5}$  and  $\alpha_H = 200$ .

**Summary** - In summary, an USOC is observed when the EDF is cooled down below 10K. An unequally spaced wavelength sequence can be generated by a variety of mechanisms, including Brillouin scattering, gain and loss grating (due to back reflection at the splicing points at both ends of the EDF), and lasing without population inversion. However, for all these cases, the theoretically predicted sequences were found to be inconsistent with the experimental results. Open loop measurements and theoretical results are presented to support the hypothesis that intermode coupling is the underlying mechanism responsible for the USOC formation. An intriguing connection between  $\{\lambda_k\}$  and the sequence of prime numbers is discussed in the SM. Future work will be devoted to explore the interplay between USOC formation, hole burning and external injection. The extremely high stability of the USOC can be exploited for some novel applications.

This work was supported by the Israeli science foundation. Preliminary measurements of a device similar to the one under study in this paper have been performed by A. Becker together with EB (these measurements are not included in this paper). The data that support the findings of this study are available from the corresponding author upon reasonable request.



- 
- [1] A. Kobayakov, M. Sauer, and D. Chowdhury, "Stimulated brillouin scattering in optical fibers," *Advances in optics and photonics*, vol. 2, no. 1, pp. 1–59, 2010.
  - [2] J. Le Gouët, J. Oudin, P. Perrault, A. Abbes, A. Odier, and A. Dubois, "On the effect of low temperatures on the maximum output power of a coherent erbium-doped fiber amplifier," *Journal of Lightwave Technology*, vol. 37, no. 14, pp. 3611–3619, 2019.
  - [3] O. Anderson and H. Bömmel, "Ultrasonic absorption in fused silica at low temperatures and high frequencies," *Journal of the American Ceramic Society*, vol. 38, no. 4, pp. 125–131, 1955.
  - [4] A. S. Pine, "Brillouin scattering study of acoustic attenuation in fused quartz," *Physical Review*, vol. 185, no. 3, p. 1187, 1969.
  - [5] M. Nikles, L. Thevenaz, and P. A. Robert, "Brillouin gain spectrum characterization in single-mode optical fibers," *Journal of Lightwave Technology*, vol. 15, no. 10, pp. 1842–1851, 1997.
  - [6] L. Thevenaz, A. Fellay, M. Facchini, W. Scandale, M. Nikles, and P. A. Robert, "Brillouin optical fiber sensor for cryogenic thermometry," in *Smart Structures and Materials 2002: Smart Sensor Technology and Measurement Systems*, vol. 4694. International Society for Optics and Photonics, 2002, pp. 22–27.
  - [7] A. Antuzevics, "Epr characterization of erbium in glasses and glass ceramics," *Low Temperature Physics*, vol. 46, no. 12, pp. 1149–1153, 2020.
  - [8] H. Haken, *Laser light dynamics*. North-Holland Amsterdam, 1985, vol. 2.
  - [9] M. Aubry, L. Mescia, A. Morana, T. Robin, A. Laurent, J. Mekki, E. Marin, Y. Ouerdane, S. Girard, and A. Boukenter, "Temperature influence on the radiation responses of erbium-doped fiber amplifiers," *physica status solidi (a)*, vol. 218, no. 15, p. 2100002, 2021.
  - [10] J. P. L. Pizzaia, R. L. Silva, A. G. Leal-Junior, and C. E. S. Castellani, "Temperature sensor based on an erbium-doped fiber sagnac interferometer," *Applied Optics*, vol. 61, no. 9, pp. 2352–2356, 2022.
  - [11] J. Moloney and A. Newell, *Nonlinear optics*. CRC Press, 2018.
  - [12] N. Kagi, A. Oyobe, and K. Nakamura, "Temperature dependence of the gain in erbium-doped fibers," *Journal of lightwave technology*, vol. 9, no. 2, pp. 261–265, 1991.
  - [13] P. Franco, M. Midrio, A. Tozzato, M. Romagnoli, and F. Fontana, "Characterization and optimization criteria for filterless erbium-doped fiber lasers," *JOSA B*, vol. 11, no. 6, pp. 1090–1097, 1994.
  - [14] E. Desurvire and J. R. Simpson, "Evaluation of 4 i 15/2 and 4 i 13/2 stark-level energies in erbium-doped aluminosilicate glass fibers," *Optics letters*, vol. 15, no. 10, pp. 547–549, 1990.
  - [15] E. Desurvire, J. Zyskind, and J. Simpson, "Spectral gain holeburning at 1.53  $\mu$ m in erbium-doped fiber amplifiers," *IEEE Photon. Technol. Lett.*, vol. 2, no. 4, pp. 246–248, 1990.
  - [16] J. Zyskind, E. Desurvire, J. Sulhoff, and D. Di Giovanni, "Determination of homogeneous linewidth by spectral gain hole-burning in an erbium-doped fiber amplifier with geo/sub 2: Sio/sub 2/core," *IEEE Photonics technology letters*, vol. 2, no. 12, pp. 869–871, 1990.
  - [17] R. Macfarlane, Y. Sun, P. Sellin, and R. Cone, "Optical decoherence in er 3+-doped silicate fiber: evidence for coupled spin-elastic tunneling systems," *Physical review letters*, vol. 96, no. 3, p. 033602, 2006.
  - [18] L. Veissier, M. Falamarzi, T. Lutz, E. Saglamyurek, C. W. Thiel, R. L. Cone, and W. Tittel, "Optical decoherence and spectral diffusion in an erbium-doped silica glass fiber featuring long-lived spin sublevels," *Physical Review B*, vol. 94, no. 19, p. 195138, 2016.
  - [19] I. L. Rittner and P. M. Krummrich, "Measurement procedure for the inverse spectral hole burning characteristics of erbium-doped fiber amplifiers (edfa)," in *Photonic Networks; 22th ITG Symposium*. VDE, 2021, pp. 1–6.
  - [20] B. K. Nayak and E. Buks, "Polarization-selective magneto-optical modulation," *Journal of Applied Physics*, vol. 132, no. 19, p. 193905, 2022.
  - [21] H. A. Haus, "Mode-locking of lasers," *IEEE Journal of Selected Topics in Quantum Electronics*, vol. 6, no. 6, pp. 1173–1185, 2000.
  - [22] T. Chu, P. Wang, and C. Zhu, "Modeling of active fiber loop ring-down spectroscopy considering gain saturation behavior of edfa," *Journal of Lightwave Technology*, vol. 38, no. 4, pp. 966–973, 2020.
  - [23] R. A. Perez-Herrera, M. Lopez-Amo, S. Harun, and H. Arof, "Multi-wavelength fiber lasers," in *Current Developments in Optical Fiber Technology*. In-Tech, 2013.
-

# Supplemental Materials: Low temperature spectrum of a fiber loop laser

Eyal Buks

Andrew and Erna Viterbi Department of Electrical Engineering, Technion, Haifa 32000 Israel

The unequally-spaced optical comb (USOC) is measured as a function of the diode current  $I_D$  in section S1. The effect of laser injection into the loop is discussed in section S2. To study the USOC wavelength selection process, the short-time scale dynamics of the system are theoretically explored in section S3. The measured pattern of the USOC wavelength sequence  $\{\lambda_k\}$  is discussed in sections S4 and S5. We find that the observed pattern  $\{\lambda_k\}$  can be attributed to a process, in which the intermode coupling contribution to the system's total energy is minimized, under the constrain that the total optical intensity is given. An intriguing connection between  $\{\lambda_k\}$  and the sequence of prime numbers is discussed.

## S1. DIODE CURRENT

The measured optical spectrum is shown in Fig. S1 as a function of the diode current  $I_D$ . The lasing threshold occurs at  $I_D = 88\text{mA}$ .

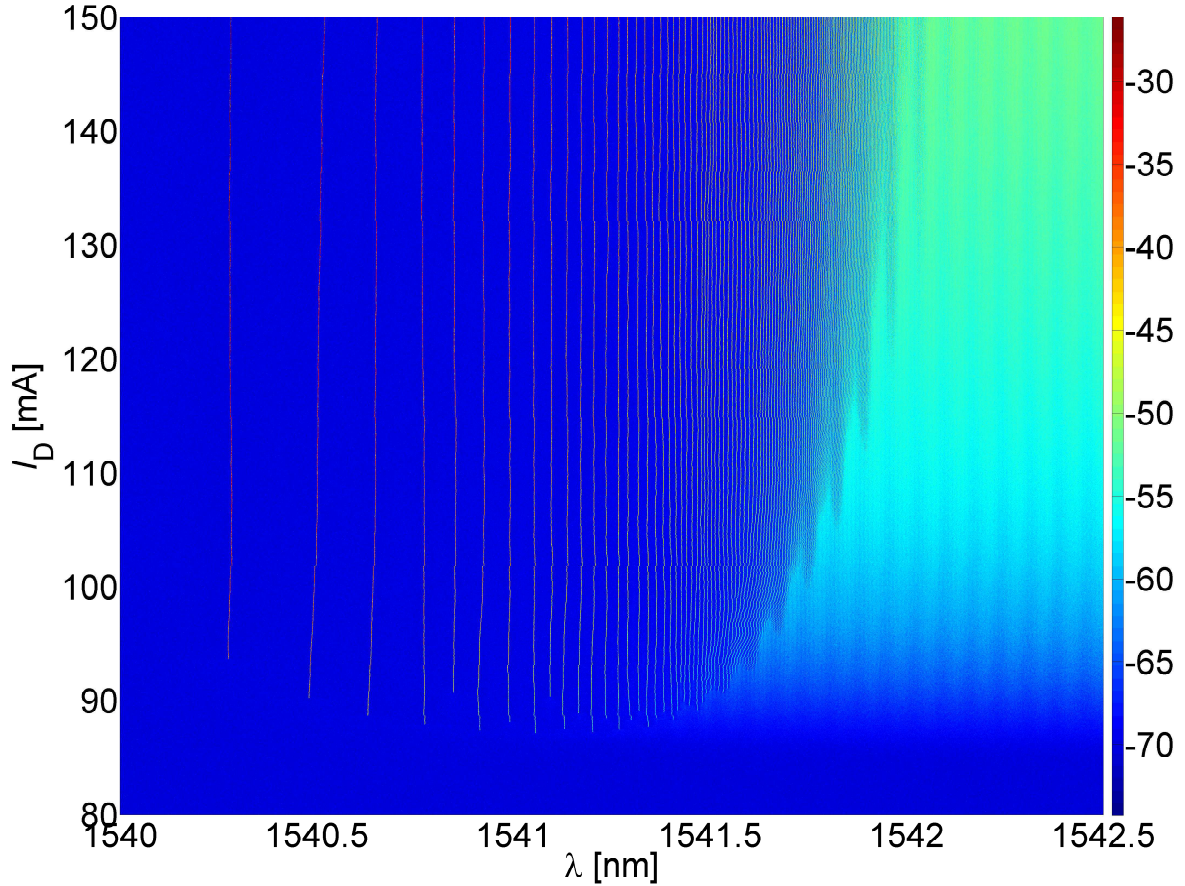


FIG. S1: The optical spectrum in dBm units as a function of diode current  $I_D$  at temperature of 2.9K.

## S2. LASER INJECTION

While the laser injection measurements that are described in the main text are performed with an open loop (see Fig. 4 of the main text), the plot in Fig. S2 below displays the effect of laser injection into the closed loop. USOC suppression near the laser wavelength of  $\lambda_L = 1541.5\text{nm}$  is attributed to the effect of gain saturation.

## S3. SHORT-TIME SCALE DYNAMICS

The optical complex amplitude at time  $t$  is expressed as  $f(f_L t)$ , where  $f_L$  is the fiber loop frequency. The function  $f(x)$  can be Fourier expanded as

$$f(x) = \sum_{n=-\infty}^{\infty} c_n e^{2\pi i n x}, \quad (\text{S1})$$

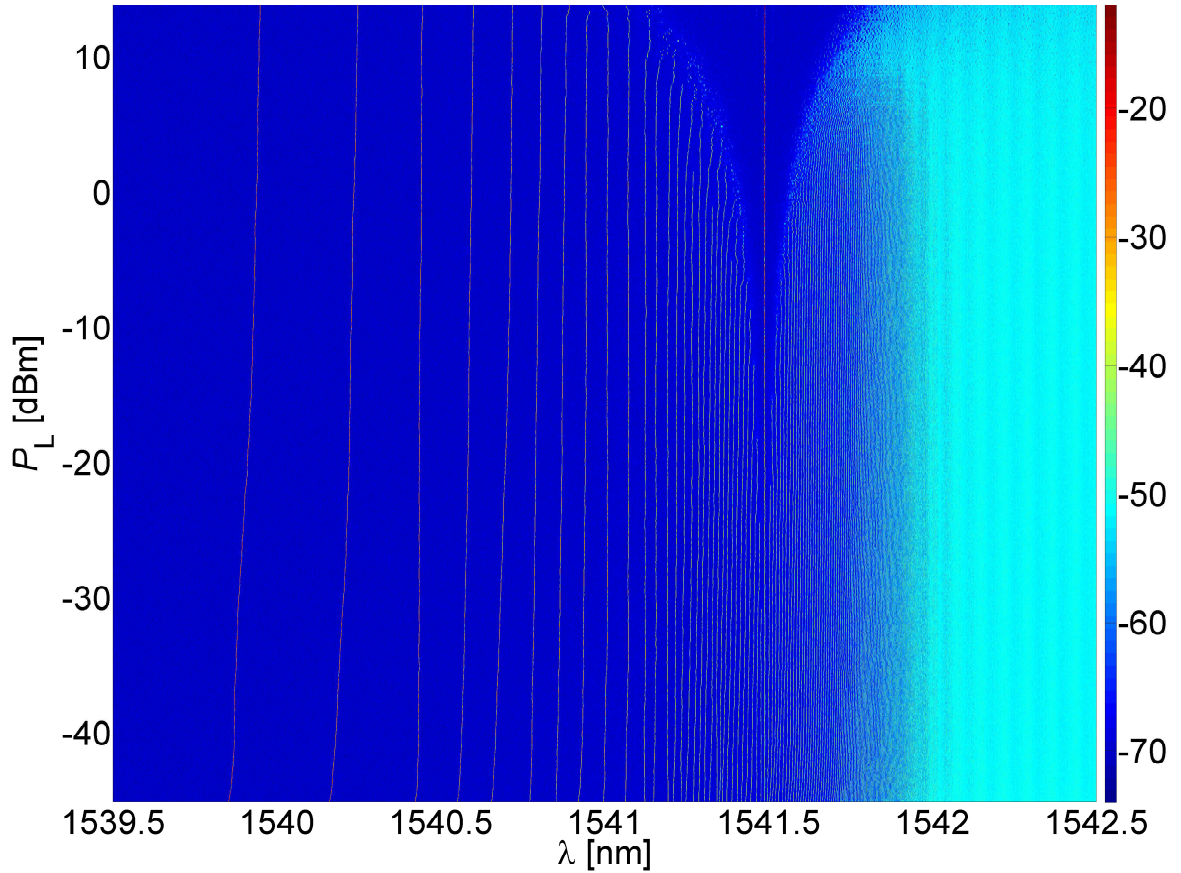


FIG. S2: Laser injection with a closed loop. The laser, having power  $P_L$  and wavelength  $\lambda_L = 1541.5\text{nm}$ , is coupled using a 5:95 optical coupler, which is connected between the points 'A' and 'B' shown in the inset of Fig. 1 of the main text. The temperature is  $T = 2.9\text{K}$ , and the diode current is  $I_D = 150\text{mA}$ .



where  $c_n$ , which is expressed as  $c_n = c'_n + ic''_n$ , where both  $c'_n$  and  $c''_n$  are real, is the complex amplitude of the  $n$ 'th mode. The  $L_p$  norm of  $f$  is given by

$$\|f\|_p = \left( \int_0^1 dx |f(x)|^p \right)^{1/p}, \quad (\text{S2})$$

and the following holds

$$\|f\|_2^2 = \sum_{n=-\infty}^{\infty} |c_n|^2 \equiv I, \quad (\text{S3})$$

where  $I$  is the total intensity, and

$$\|f\|_4^4 = \sum_{n'-n''+n'''-n''''=0} c_{n'} c_{n''}^* c_{n'''} c_{n''''}^*. \quad (\text{S4})$$

As will be discussed below, the term  $\|f\|_4^4$  plays an important role in the system's short-time dynamics. Below an upper bound imposed upon  $\|f\|_4^4$  is derived [see inequality (S9) below].

When the expansion (S1) contains a finite number of non-vanishing terms,  $f(x)$  can be expressed as

$$f(x) = \sum_{n \in N_f} c_n e^{2\pi i n x}, \quad (\text{S5})$$

where  $N_f = \{n \in \mathbb{Z} : c_n \neq 0\}$  ( $\mathbb{Z}$  denotes the set of integers), and  $\|f\|_4^4$  as [see Eq. (S4)]

$$\begin{aligned} \|f\|_4^4 &= \int_0^1 dx \left( \sum_{n', n'' \in N_f} c_{n'} c_{n''}^* e^{2\pi i (n' - n'')x} \right)^2 \\ &= \int_0^1 dx \left( \sum_d C_d e^{2\pi i d x} \right)^2, \end{aligned}$$

where

$$C_d = \sum_{\substack{n', n'' \in N_f \\ n' - n'' = d}} c_{n'} c_{n''}^*. \quad (\text{S6})$$

Note that  $C_0 = \sum_{n'} |c_{n'}|^2 = \|f\|_2^2 = I$ ,  $C_{-d} = C_d^*$  and

$$\begin{aligned} \|f\|_4^4 &= \sum_{d', d''} C_{d'} C_{d''}^* \int_0^1 dx e^{2\pi i (d' - d'')x} \\ &= \sum_d |C_d|^2. \end{aligned} \quad (\text{S7})$$

With the help of the Cauchy's Inequality one finds that [see Eq. (S6)]

$$|C_d|^2 \leq \mathcal{N}_d \sum_{\substack{n', n'' \in N_f \\ n' - n'' = d}} |c_{n'} c_{n''}^*|^2, \quad (\text{S8})$$

where  $\mathcal{N}_d = |\{(n', n'') \in N_f \times N_f : n' - n'' = d\}|$  ( $|S|$  denotes cardinality, i.e. number of members, of a given set  $S$ ), and thus [see Eqs. (S3) and (S7)]

$$\begin{aligned} \|f\|_4^4 &= |C_0|^2 + \sum_{d' \neq 0} |C_{d'}|^2 \\ &\leq \left( 1 + \max_{d \neq 0} \mathcal{N}_d \right) \|f\|_2^4. \end{aligned} \quad (\text{S9})$$

Consider the case where the term proportional to  $g_m$  in Eq. (2) in the main text can be disregarded. For this case, and when noise is taken into account, the set of coupled equations can be expressed as [see Eq. (2) in the main text]

$$\dot{c}_m = -\partial_m^* \mathcal{H} + \xi_m, \quad (\text{S10})$$

where  $\partial_m$ , which is given by

$$\partial_m = \frac{\partial}{\partial c_m} = \frac{1}{2} \left( \frac{\partial}{\partial c'_m} - i \frac{\partial}{\partial c''_m} \right), \quad (\text{S11})$$

is the Wirtinger derivative (note that  $\partial_m c_m = 1$  and  $\partial_m c_m^* = 0$ ), the Hamiltonian is given by  $\mathcal{H} = \mathcal{H}_d + \mathcal{H}_c$ , where the dispersion Hamiltonian  $\mathcal{H}_d$  is given by  $\mathcal{H}_d = -\Gamma_d \sum_{n'} n'^2 c_{n'} c_{n'}^*$ , and the intermode coupling Hamiltonian  $\mathcal{H}_c$  is given by [see Eq. (S4)]

$$\mathcal{H}_c = \frac{\Gamma_c}{2} \|f\|_4^4. \quad (\text{S12})$$

The complex white noise terms  $\xi_m = \xi'_m + i\xi''_m$ , where both  $\xi'_m$  and  $\xi''_m$  are real, satisfy the relations  $\langle \xi'_m(t) \xi'_m(t') \rangle = \langle \xi''_m(t) \xi''_m(t') \rangle = 2\tau\delta(t-t')$  and  $\langle \xi'_{m'}(t) \xi''_{m''}(t') \rangle = 0$ , where  $\tau$  is positive, and where angle brackets denote time averaging. The steady state solution of Eq. (S10) is given by Eq. (7.251) of Ref. [S2].

The above finding (S12) that  $\mathcal{H}_c$  is proportional to  $\|f\|_4^4$ , together with the upper bound given by inequality (S9), suggest that the intermode coupling contribution  $\mathcal{H}_c$  to the total Hamiltonian can be minimized (for a given total intensity  $\|f\|_2^2 = I$ ) by selecting the set of excited modes  $N_f$  such that  $\max_{d \neq 0} \mathcal{N}_d$  is minimized. In particular, the case  $\max_{d \neq 0} \mathcal{N}_d = 1$  is discussed below.

When the condition  $\max_{d \neq 0} \mathcal{N}_d = 1$  is satisfied the set  $N_f$  is said to be SU. Alternatively, the term SU can be defined as follows. Consider the equation

$$n' - n'' = n''' - n'''' , \quad (\text{S13})$$

where  $n', n'', n''', n'''' \in N_f$ . When Eq. (S13) is unsolvable, unless  $n' = n'''$  and  $n'' = n''''$ , the set  $N_f$  is said to be SU. For this case all spacings between pairs of elements belonging to  $N_f$  are unique, i.e.  $\max_{d \neq 0} \mathcal{N}_d = 1$ , and the upper bound given by inequality (S9) yields  $\mathcal{H}_c \leq \Gamma_c I^2$ .

#### S4. THE MEASURED USOC WAVELENGTH SEQUENCE $\{\lambda_k\}$

The measured USOC wavelength sequence  $\{\lambda_k\}$  is presented by Fig. 3 in the main text. The red solid line shown in Fig. 3(b) in the main text is calculated using the relation for  $k \geq 1$

$$n_k = \nu \log p_k, \quad (\text{S14})$$

where  $p_k$  is the  $k$ 'th prime number. For this measurement, the dimensionless pre-factor  $\nu$  is found by fitting to be given by  $\nu = 5721$ . The comparison between the measured values of  $i_k = (f_0 - f_k)/f_L$  and the calculated values of  $n_k$  obtained from Eq. (S14) yields a good agreement [see Fig. 3(b) in the main text]. The level of agreement is quantified by the parameter  $\varepsilon = k_m^{-1} \sum_{k=1}^{k_m} |(i_k - n_k)/i_{k_m}|$ , where  $k_m$  is the number of peaks that can be reliably resolved. For the data shown in Fig. 3) in the main text  $k_m = 150$  and  $\varepsilon = 0.004$ . The USOC shown in Fig. 3 in the main text has been obtained in a slow cooling process with a fixed applied diode current  $I_D$ . Note that larger deviation between data and Eq. S14 is observed in other cases. One example is a USOC that is obtained by switching off, and then abruptly switching on, the diode current  $I_D$ , while keeping the temperature at its base value. For this case typically  $\varepsilon \simeq 0.01$ .

#### S5. RU AND SU SETS

The above-discussed experimental finding that  $i_k = (f_0 - f_k)/f_L \simeq n_k$ , where  $n_k$  is given by Eq. (S14), implies that the set  $N_f$  of excited mode indices corresponding to the measured USOC is nearly SU [recall the fundamental theorem of arithmetic, and that  $\log x + \log y = \log(xy)$ ]. As was shown above, this observation suggests that the USOC wavelength sequence is selected in a way that minimizes the energy associated with intermode coupling (for a given total intensity  $I$ ). On the other hand, other USOC wavelength sequences can give rise to other SU sets  $N_f$ . Below we show that for a given width of the lasing band, the number of peaks of the experimentally observed USOC

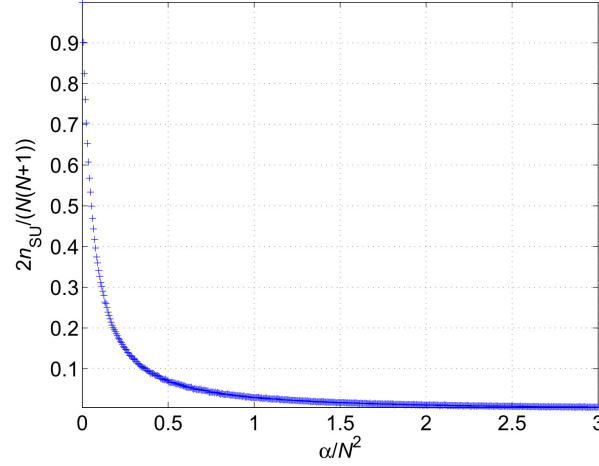


FIG. S3: A plot of  $2n_{\text{SU}}/(N(N+1))$  as a function of  $\nu/N^2$  for the case  $N = 1500$ .

has the same order of magnitude as the largest possible number. The analysis below also addresses the question what determines the value of the dimensionless coefficient  $\nu$  in Eq. (S14).

A set  $A = \{e_1, e_2, \dots, e_N\}$  is said to be RU if all ratios between pairs of elements belonging to  $A$  are unique, i.e. if the equation  $e_{n'}/e_{n''} = e_{n'''} / e_{n''''}$  is unsolvable, unless  $n' = n'''$  and  $n'' = n''''$ . Similarly, as was already defined above, a set  $A = \{e_1, e_2, \dots, e_N\}$  is said to be SU if all spacings between pairs of elements belonging to  $A$  are unique, i.e. if the equation  $e_{n'} - e_{n''} = e_{n'''} - e_{n''''}$  is unsolvable, unless  $n' = n'''$  and  $n'' = n''''$ .

The set  $A_p = \{p_1, p_2, p_3, p_4, \dots, p_N\}$  of the first  $N$  prime numbers is RU (the  $n$ 'th prime number is denoted by  $p_n$ ). The set  $A_p$  can be used for the generation of an SU set  $A_g = \{\log p_1, \log p_2, \dots, \log p_N\}$ . The set of real numbers  $A_g$  can be mapped into a set of integers  $A_{gi} = \{a_1, a_2, \dots, a_N\}$ , where

$$a_n = \lfloor \nu \log p_n + 1/2 \rfloor, \quad (\text{S15})$$

and where  $\nu > 0$  is a constant ( $\lfloor x + 1/2 \rfloor$  is the nearest integer to  $x$ , where  $\lfloor x \rfloor$  is the floor of  $x$ ).

For what values of  $\nu$  the set  $A_{gi}$  becomes SU? Let  $S_{gi} = \{a_{n'} - a_{n''} | N \geq n' > n'' \geq 1\}$  be the set of positive spacings between pairs of elements belonging to  $A_{gi}$ . The integer  $n_{\text{SU}}$  is defined by

$$n_{\text{SU}} = \frac{N(N+1)}{2} - |S_{gi}|. \quad (\text{S16})$$

When  $n_{\text{SU}} = 0$  the set  $A_{gi}$  is SU. A plot of  $2n_{\text{SU}}/(N(N+1))$  as a function of  $\nu/N^2$  is shown in Fig. S3. The plot in Fig. S3 suggests that for  $\nu \gtrsim N^2$  the set  $A_{gi}$  becomes SU. The relation  $\nu = N^2$  together with the number of observed USOC peaks  $\simeq 150$  yields the value of 22500 for  $\nu$ . This rough estimate is about 3.9 times the value of  $\nu = 5721$  that is extracted from the fit between data and Eq. S14 (see Fig. 3 in the main text).

As was shown above, the experimentally observed USOC yields the SU set  $A_{gi}$  given by Eq. (S15) [compare with Eq. S14]. For the general case, a comb can be characterized by the number of peaks within the lasing bandwidth, which depends on the packing factor  $\chi$  of the corresponding SU set of integers. Below we define the packing factor  $\chi$ , derive an upper bound for  $\chi$ , and compare the bound with the packing factor  $\chi(A_{gi})$  of the SU set  $A_{gi}$ . As is shown below,  $\chi(A_{gi})$  has the same order of magnitude as the largest possible value of  $\chi$  of any SU set having the same number  $N$  of elements.

The integer  $a_n \in A_{gi}$  (S15) can be expressed as

$$a_n = \nu \log p_n + \epsilon_n, \quad (\text{S17})$$

where  $|\epsilon_n| \leq 1/2$ . The equation  $a_{n'} - a_{n''} = a_{n'''} - a_{n''''}$  can be rewritten as

$$0 = \nu \log \varrho + \varepsilon, \quad (\text{S18})$$

where  $\varrho = (p_{n'}/p_{n''}) / (p_{n'''} / p_{n''''})$ , and where  $\varepsilon$ , which is given by  $\varepsilon = \epsilon_{n'} - \epsilon_{n''} - \epsilon_{n'''} + \epsilon_{n''''}$ , is bounded by  $|\varepsilon| \leq 2$ . Consider a nontrivial solution of Eq. (S18), i.e. a solution for which  $\varrho \neq 1$ . Without loss of generality, it is assumed



that  $\varrho > 1$ , i.e.  $p_{n'}p_{n'''} > p_{n''}p_{n''''}$ . Since  $p_n$  are all integers, this implies that  $p_{n'}p_{n'''} - p_{n''}p_{n''''} \geq 1$ . By using the relation  $\varrho - 1 = (p_{n'}p_{n'''} - p_{n''}p_{n''''}) / (p_{n''}p_{n''''})$  one finds that  $\varrho = 1 + \varrho - 1 \geq 1 + 1 / (p_{n''}p_{n''''}) \geq 1 + p_N^{-2}$ . Thus  $|\log \varrho| \geq p_N^{-2}$  (it is assumed that  $N \gg 1$ ), hence  $A_{\text{gi}}$  is SU provided that  $\nu \geq 2p_N^2$ .

According to the prime number theorem, for  $n \geq 6$  the following holds [S1]

$$\zeta_n - \frac{1}{2} < \frac{p_n}{n} < \zeta_n + \frac{1}{2}, \quad (\text{S19})$$

where  $\zeta_n = \log n + \log \log n - 1/2$ . Using the approximation [see inequality (S19)]

$$p_n \simeq n\zeta_n, \quad (\text{S20})$$

one finds for the case  $\nu = 2p_N^2$  that

$$a_N \simeq 2N^2\zeta_N^2 \log(N\zeta_N). \quad (\text{S21})$$

For a general SU set of integers  $A = \{a_1, a_2, \dots, a_N\}$ , where  $1 \leq a_1 < a_2 < \dots < a_N$ , the packing factor  $\chi(A)$  is defined by  $\chi(A) = N/a_N$ . An upper bound upon  $\chi(A)$  is derived below. For a given positive integer  $d$ , let  $S_d$  be the number of pairs  $(a_{n'}, a_{n''}) \in A^2$  such that  $a_{n''} - a_{n'} = d$ . Since  $A$  is SU,  $S_d \in \{0, 1\}$  for any positive integer  $d$ . The number of distinct positive integers  $d$ , such that  $S_d = 1$  is  $N(N-1)/2$  (i.e. the number of ordered pairs of distinct element in  $A$ ). On the other hand,  $a_{n''} - a_{n'} \leq a_N - 1$  for any  $a_{n'}, a_{n''} \in A$ , and thus  $N(N-1)/2 \leq a_N - 1$ . This condition imposes an upper bound upon the packing factor

$$\chi(A) \leq \frac{1}{\frac{N}{2} - \frac{1}{2} + N^{-1}}. \quad (\text{S22})$$

This bound can be compared with the packing factor of the SU set  $A_{\text{gi}}$ , which for the case  $\nu = 2p_N^2$  is given by [see Eq. (S21)]

$$\chi(A_{\text{gi}}) \simeq \frac{1}{2N\zeta_N^2 \log(N\zeta_N)}. \quad (\text{S23})$$

Hence, to leading order  $\chi = O(N^{-1})$  for both the upper bound (S22) and for the set  $A_{\text{gi}}$  (S23). In other words, for large  $N$  the packing factor of the SU set  $A_{\text{gi}}$  has the same order of magnitude as the largest possible packing factor.

[S1] Pierre Dusart, "The  $k$  th prime is greater than  $k(\ln k + \ln \ln(k-1))$  for  $k > 2$ ", Mathematics of computation, 411–415 (1999).

[S2] Eyal Buks, "Statistical physics - Lecture Notes", <http://buks.net.technion.ac.il/teaching/> (2022).